ChemComm



COMMUNICATION

View Article Online



Cite this: DOI: 10.1039/d0cc03713c

Received 25th May 2020, Accepted 29th June 2020

DOI: 10.1039/d0cc03713c

rsc.li/chemcomm

Quinoxaline radical-bridged transition metal complexes with very strong antiferromagnetic coupling†

A new family of radical-bridged compounds, $(Cp*_2Co)[M_2Cl_4(dpq)]$ (M = Fe (1), Co (2), Zn (3)), (dpq = 2,3-di(2-pyridyl)-quinoxaline) is reported. Magnetic studies, DFT and *ab initio* calculations reveal strong antiferromagnetic metal-radical interactions with coupling constants of J = -213.1 and -218.8 cm⁻¹ for 1 and 2, respectively.

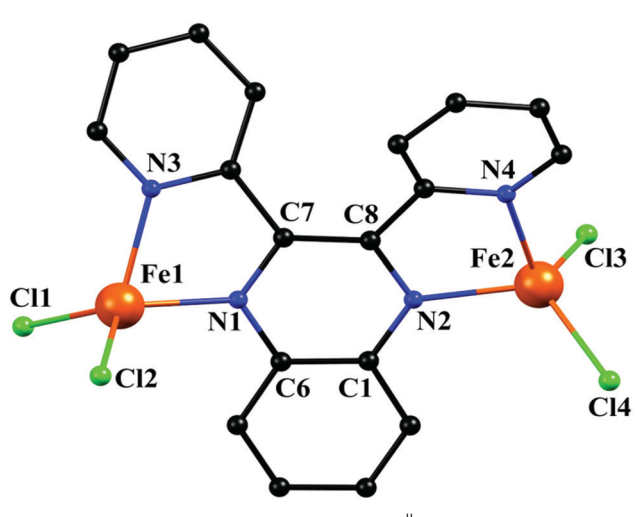
Molecular magnetic materials¹ are of paramount interest for many technological applications including high density data storage,² molecular electronic devices,³ and quantum computation.4 The syntheses of these materials often rely on self-assembly reactions between paramagnetic metal ions and organic bridging ligands which offer the advantages of thermodynamic stability, solubility, and crystallinity. The success of this approach notwithstanding, the presence of closed-cell bridging ligands often limits the properties and dynamics of magnetic materials, leading to competing magnetic interactions, moderate-to-weak magnetic coupling, and low-lying excited states, among others. A successful strategy to overcome these obstacles is to use organic radicals as bridging ligands between metal spin centers which leads to stronger direct magnetic coupling as compared to the indirect superexchange interactions observed in the case of diamagnetic linkers.⁵ Indeed, a number of interesting radical bridged transition metal and lanthanide complexes have been reported to date, including the $[K(18\text{-crown-6})(THF)_2][\{[(Me_3Si)_2N]_2(THF)Ln\}_2]$ $(\mu-\eta^2:\eta^2-N_2)$] compound that exhibits magnetic hysteresis up to 14 K^6 as well as the complex $[(TPyA)_2Fe_2(^{NPh}L)](SO_3CF_3)$ (TPyA =tris(2-pyridylmethyl)-amine, NPhLH₂ = N,N',N",N"''-tetraphenyl-2,5-diamino-1,4-diiminobenzoquinone)⁷ which exhibits a coupling constant of 900 cm⁻¹. In general, however, radical bridged metal complexes have been far less studied and in many ways

Department of Chemistry, Texas A&M University, College Station, Texas 77842-3012, USA. E-mail: dunbar@chem.tamu.edu are in their infancy than examples bridged by innocent closedshell ligands.

Research in our group has focused on the design of metal complexes bearing the radical forms of tetrazine-based ligands, including 3,6-bis(pyridyl)-1,2,4,5-tetrazine (bptz) and 3,6bis(pyrimidyl)-1,2,4,5-tetrazine (bmtz). The implementation of these ligands in both 3d and 4f metal chemistry has afforded structurally interesting compounds including bimetallic species as well as supramolecular architectures.8 Recently, we turned our attention to other, relatively unexplored, non-innocent ligands that can undergo redox chemistry to stabilize radical isomers. Taking into account its bridging capabilities, 9 together with its reversible electrochemical reduction at −1.95 V versus Fc/Fc⁺ in MeCN (Fig. S2, ESI†), we investigated reduced bimetallic transition metal complexes of the 2,3-di(2-pyridyl)-quinoxaline (dpq). Herein, we report the syntheses, structures and magnetic properties of three new bimetallic complexes, viz., (Cp*2Co)[M2Cl4(dpq)] (M = Fe(1), Co(2), and Zn(3)). To the best of our knowledge, these compounds are the first examples in which the dpq ligand is in its radical anion form.

Compounds 1-3 were prepared by the reaction of anhydrous MCl₂ (M = Fe, Co, Zn) and dpg in a 2:1 molar ratio in the presence of 1 equivalent of the reducing agent Cp*2Co in MeCN. Layering of the resulting solutions with Et₂O afforded crystals suitable for X-ray analyses in high yields of 55-75%. Complexes 1-3 are isostructural, thus only the structure of 1 will be described as a representative example. The molecular structure of the anion in 1 (Fig. 1) consists of two crystallographically inequivalent Fe atoms linked by a bridging dpq ligand. Each metal is four-coordinate with a distorted tetrahedral geometry. Two coordination sites are occupied by a chelating N-donor dpq ligand with the remaining two being filled by two terminal Cl⁻ ions. The geometries¹⁰ for Fe1 and Fe2 in 1 exhibit average dihedral angles of 76.5° and 77.0° which further supports the fact that each Fe is in a distorted tetrahedral geometry. Complexes 2 and 3 exhibit similar dihedral angles (77.9° for Co1/Co2, 78.3° for Zn1 and 78.2° for Zn2). The

[†] Electronic supplementary information (ESI) available: Synthetic, Crystallographic, Magnetic and Computational details. CCDC 2005075-2005077. For ESI and crystallographic data in CIF or other electronic format see DOI: 10.1039/d0cc03713c



Communication

Fig. 1 Labeled representation of **1**. Colors: Fe^{II}, orange; N, blue; C, black, Cl, green. Hydrogen atoms are omitted for the sake of clarity.

oxidation state of the Fe atoms is established as 2+ by charge balance considerations and bond valence sum (BVS) 11 calculations (ESI†). The dpq ligand is considerably distorted; the two pyridine rings are twisted by 28.9° and 25.6° (28.4° and 24.2° in 2; 28.3° and 25.9° in 3) with respect to the mean plane of the quinoxaline group, which is also distorted.

A close inspection of the quinoxaline C–C (C1–C6, C7–C8) and C–N (N1–C6, N1–C7, N2–C1, N2–C8) bond distances in 1–3 revealed average distances of 1.403(5) Å and 1.372(5) Å, respectively. These values deviate significantly from the reported values for the neutral dpd ligand (C–C: $\sim 1.423(4)$ and C–N: $\sim 1.344(4)$), $^{9a-c}$ reflecting the net decrease in C–C bond order and a net increase in C–N bond order. These parameters are indicative of the presence of an additional electron in the ligand molecular orbitals, which is further supported by the short M–N_{pz} distances (M = Fe: 2.043(2), Co: 1.966(3), Zn: 2.022(4)) observed in 1–3, consistent with a strong metal–ligand interaction. Additionally, the solid-state X-band EPR spectrum of the Zn analogue 3 at 293 K, shown in Fig. 2, features a single resonance centered on g = 2.0046, confirming the presence of the dpq radical.

Solid-state direct-current (dc) magnetic susceptibility ($\gamma_{\rm M}$) data on dried and analytically pure samples of 1 and 2 were collected in the 2-300 K range at an applied field of 0.1 T and are plotted as $\chi_{M}T$ vs. T in Fig. 3. For 1, the experimental $\chi_{M}T$ value (7.63 cm³ K mol⁻¹) at 300 K is considerably higher than the theoretical value of 6.38 cm³ K mol⁻¹ for two noninteracting high-spin, S = 2, Fe^{II} ions and one S = 1/2 dpq radical (g = 2.0), due to spin-orbit coupling contributions.¹² Upon cooling, the $\chi_{\mathbf{M}}T$ product increases gradually to a value of 8.41 cm³ K mol⁻¹ at 75.0 K. Below this temperature $\chi_{\rm M}T$ decreases sharply to a value of 1.03 cm³ K mol⁻¹ at 2.0 K. The $\chi_{\rm M}T$ value at 75 K is very close to that expected for an S=7/2ground state (8.35 cm³ K mol⁻¹, g = 2.06), arising from strong antiferromagnetic metal-radical interactions, while the low temperature decrease can be attributed to zero-field splitting as well as antiferromagnetic inter- or intra-molecular metal-metal interactions.

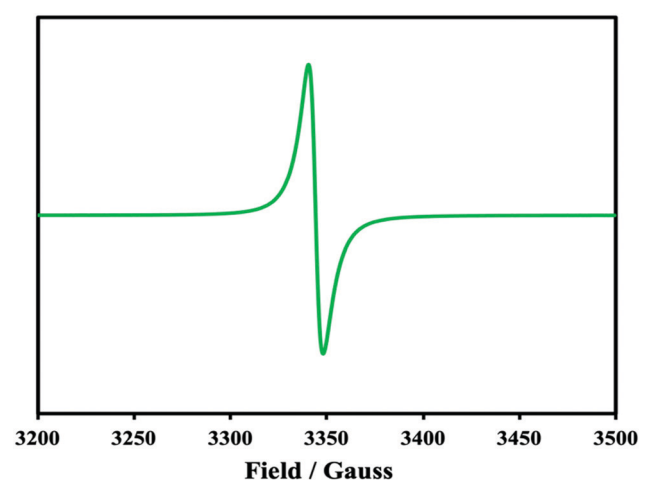


Fig. 2 Solid-state X-band EPR spectrum of **3** at 293 K with microwave frequency 9.390 GHz.

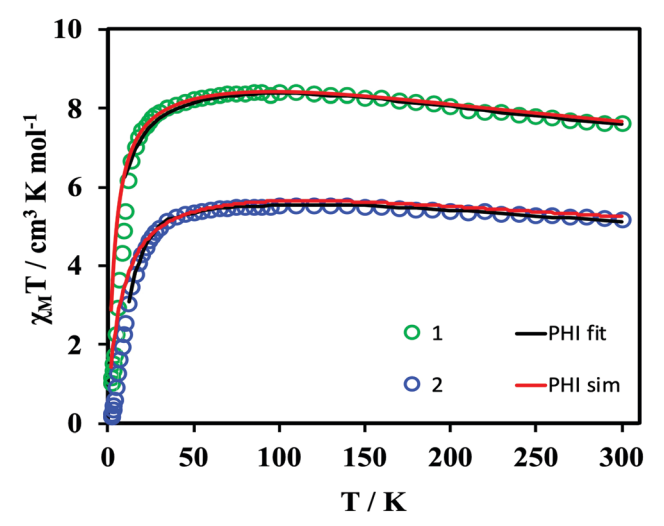


Fig. 3 $\chi_{\text{M}}T$ vs. T plots for **1** and **2**. Black lines represent fit of the experimental data according to spin Hamiltonian described in the text. Red curves represent simulations based on DFT data.

Complex 2 exhibits similar behavior, with $\chi_{\rm M}T$ slightly increasing from 5.19 cm³ K mol⁻¹ at 300 K to a maximum of 5.48 cm³ K mol⁻¹ at 75 K, and then sharply decreasing to 0.28 cm³ K mol⁻¹ at 2.0 K. The 300 K value for 2 is higher than the spin-only (g=2) value of 4.13 cm³ K mol⁻¹ for two non-interacting high spin Co^{II} ions (S=3/2) and one dpq radical (S=1/2), which reflects strong orbital angular momentum contributions. The shape of the curve indicates dominant antiferromagnetic exchange interactions between the Co^{II} ions and the dpq radical corresponding to a ferrimagnetic S=5/2 ground state for 2. Also, the reduced magnetization data for 1 and 2 (Fig. S4 and S5, ESI†) indicate significant D values for both complexes and/or population of low-lying excited states since the isofield lines do not superimpose onto a single master curve.

To estimate the metal-radical magnetic exchange interactions in 1 and 2, the magnetic susceptibility data above 10 K

were fit using the PHI program¹³ according to the following spin Hamiltonian:

$$\begin{split} \hat{H} &= -2J_{1} \big[\hat{S}_{\text{rad}} \cdot \big(\hat{S}_{\text{M1}} + \hat{S}_{\text{M2}} \big) \big] - 2J_{2} \big(\hat{S}_{\text{M1}} \cdot \hat{S}_{\text{M2}} \big) \\ &+ D \Bigg[\sum_{M=1}^{2} \left(\hat{S}_{z,M}^{2} - \frac{1}{3} \hat{S}_{M}^{2} \right) \Bigg] \\ &+ \mu_{\text{B}} g_{\text{M}} \big(\hat{S}_{\text{M1}} + \hat{S}_{\text{M2}} \big) H + \mu_{\text{B}} g_{\text{rad}} \hat{S}_{\text{rad}} H \end{split}$$

where J_1 and J_2 are the \mathbf{M}^{II} -radical and the \mathbf{M}^{II} - \mathbf{M}^{II} exchange coupling constants, with MII = Fe and Co, for 1 and 2, respectively. The third term represents the M^{II} axial zero-field splitting, D, while the last two terms account for the Zeeman interactions, including both the M^{II} and the radical contributions. The best fit gave the following parameters: $J_1 = -218.8 \text{ cm}^{-1}$, $J_2 =$ $+1.0 \text{ cm}^{-1}$, $D_{\text{Fe}} = +9.85$, and $g_{\text{Fe}} = 2.09 \text{ for 1, and } J_1 = -213.1 \text{ cm}^{-1}$, $J_2 = +2.5 \text{ cm}^{-1}$, $D_{\text{Co}} = +18.04$, and $g_{\text{Co}} = 2.50 \text{ for } 2$.

The fitting results reveal weak ferromagnetic MII-MII coupling and strong antiferromagnetic MII-radical exchange interactions. Note that the value of the Co^{II}-dpq radical exchange in 2 is lower than the values obtained using phenazine ($\sim -500 \text{ cm}^{-1}$), ¹⁴ tetraazalene (-396 cm⁻¹)¹⁵ or hexaazatrinaphthylene-based (-290 cm⁻¹)¹⁶ radicals but considerably higher than those reported using nindigo-based (-137 cm⁻¹), ¹⁷ bptz (-67.5 cm⁻¹), ^{8d} oxazolidine nitroxide (-63.5 cm^{-1}) , ¹⁸ bmtz (-62.5 cm^{-1}) ^{8a} or chloranilate (-52 cm⁻¹)19 radicals. The Fe^{II}-dpq radical coupling is larger than that observed for the tetraoxolene (-57 to)-65 cm⁻¹)²⁰ or chloranilate (+19 cm⁻¹)¹⁹ radicals but smaller than that reported for the tetraazalene $(>900 \text{ cm}^{-1})^7$ or oxazolidine nitroxide $(-315 \text{ cm}^{-1})^{18}$ radicals. The large and positive D and g > 2 values obtained for the Fe^{II} and Co^{II} compounds are in good agreement with values reported for other tetrahedral Fe^{II} and Co^{II} ions.²¹ Attempts to fit the data in the 2.0-300 K region were unsuccessful due to the precipitous decline below 10 K. The inclusion of an intermolecular zJ interaction (including and excluding J_2) did not improve the fitting and gave unreasonable values for J_1 , J_2 , D, and g parameters.

Using Density Functional Theory (DFT) and ab initio CASSCF (Complete Active Space Self-Consistent Field) calculations, the magnetic exchange interactions (I), and g and D parameters were computed (see Computational details in ESI†). DFT calculations were performed by using B3LYP functionals²² to compute the neighboring exchange interaction between metal-radical centers and the next neighboring exchange interaction between metal centers in both complexes. The $J_{\mathbf{M}^{\mathrm{II}}$ -rad values were calculated to be -224.3 cm⁻¹ and -242.4 cm⁻¹ and the $J_{M^{II}-M^{II}}$ values were computed to be +2.1 cm⁻¹ and +2.4 cm⁻¹ for 1 and 2, respectively (Tables S4 and S5, ESI†). The calculations reproduce the sign of the experimentally determined magnetic coupling values very well, but the magnitude is slightly overestimated. DFT computed I values confirm spin ground states of S = 7/2 and S = 5/2 for 1 and 2, respectively which arise when the M^{II} ions have spin-up configurations and the dpq radical has a spin-down configuration (Fig. 4, top). In both the complexes, the unpaired electron from the t_2 magnetic orbital of M^{II} ion overlaps with the π^* orbital of

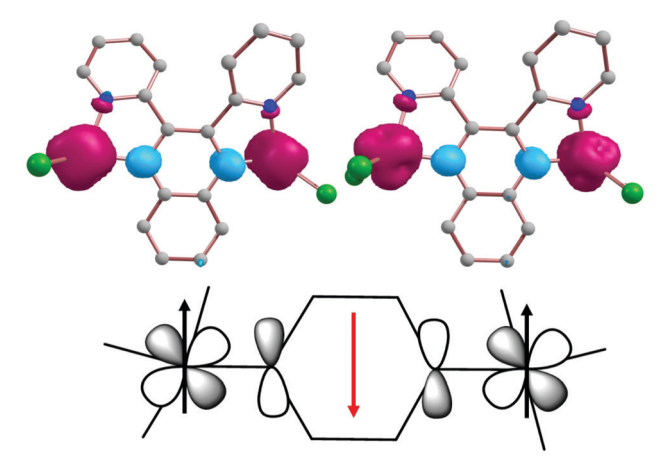


Fig. 4 DFT computed spin density plots for (top left) 1 and (top right) 2. The red and blue isodensity surfaces (0.0043 e⁻ Bohr⁻³) indicate positive and negative spin phases, respectively. (bottom) Molecular Orbital (MO) diagram showing the antiferromagnetic interactions between radical and Fe^{II}/Co^{II} centers in 1 and 2.

the dpg radical (Fig. 4, bottom) which leads to the strong antiferromagnetic coupling between them.8d

To further understand the observed magnetic behavior in 1 and 2, the g and D parameters of the Fe^{II} and a Co^{II} ions were computed using ab initio CASSCF calculations. The CASSCF calculations yielded g values of 2.10 and 2.38, D values of 8.2 cm^{-1} and 18.7 cm^{-1} , and E/D values of 0.17 and 0.08 for an Fe^{II} and a Co^{II} ion in 1 and 2, respectively. The computed g and D values are in good agreement with the experimentally determined parameters and are in the range of values expected for anisotropic Fe^{II} and Co^{II} ions. 8d,15,19 Using the eigenvalue plots, the calculated sign and magnitude of the D value of a Fe^{II}/Co^{II} ion in 1 and 2 were rationalized (see Fig. 5). The orbital splitting pattern indicates a spin-allowed excitation of a β-electron between the orbitals with different $|\pm m_1|$ levels $(d_{x^2-y^2} \rightarrow d_{z^2} \text{ for the Fe}^{II} \text{ ion and } d_{z^2} \rightarrow d_{yz} \text{ for the Co}^{II} \text{ ion)},$ which leads to a positive D value for these ions.²³ The major positive contribution to the D value is from the first four quintet and quartet excited states for the FeII and the CoII ions, respectively (Table S6, ESI†). For the CoII ion in 2, the energy gap between the ground and the first excited state is large (1853.8 cm⁻¹) compared to the Fe^{II} ion in **1** (1707.2 cm⁻¹). Thus, the positive *D* contribution is significantly larger for the Co^{II} ion compared to the Fe^{II} ion due to this very low-lying first excited state, whereas the other excited states marginally contribute to the total positive D value.

In summary, the new family of compounds (Cp*2Co) $[M_2Cl_4(dpq)]$ (M = Fe, Co, Zn) is reported. The presence of the ligand-centered radical was confirmed by X-ray crystallography, SQUID magnetometry, and EPR spectroscopy. In these complexes, which are the first ones based on the radical form of the dpq ligand, the metal ions are four-coordinate with tetrahedral geometries. Both complexes 1 and 2 exhibit strong antiferromagnetic metal radical coupling, as evidenced by the large negative coupling constants. DFT and ab initio computed spin-Hamiltonian parameters are in good agreement with the experimentally Communication ChemComm

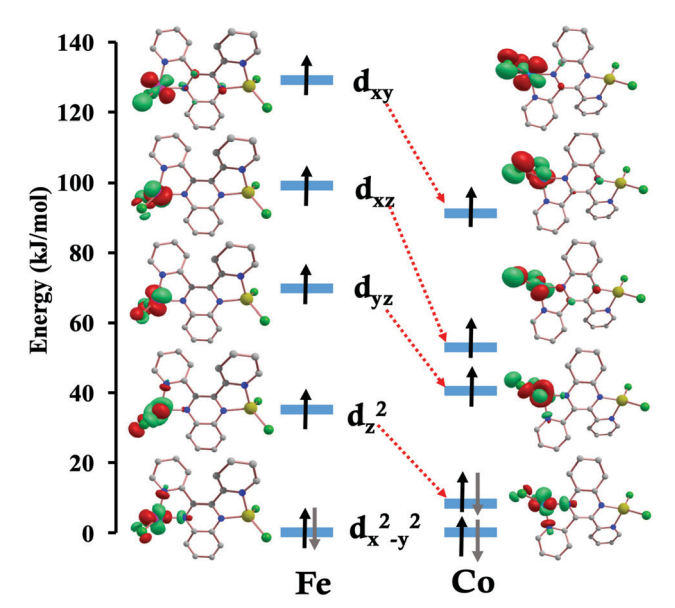


Fig. 5 $\,$ Ab initio computed d-orbital ordering for Fe^{II} and Co^{II} ions in **1** and **2**, respectively.

determined values and they nicely reproduce the magnetic susceptibility data. Further studies involving the coordination geometry of 3d- or 4f-metal ions with this and other structurally similar ligands will be reported in due course.

We gratefully acknowledge support for this work by the National Science Foundation (CHE-1808779) and the Robert A. Welch Foundation (Grant A-1449). The SQUID magnetometer was purchased with funds provided by the Texas A&M University Vice President of Research. We would like to thank the HPRC at Texas A&M University for providing computing resources.

Conflicts of interest

There are no conflicts to declare.

Notes and references

- 1 (a) G. Christou, D. Gatteschi, D. N. Hendrickson and R. Sessoli, MRS Bull., 2000, 25, 66–71; (b) R. Bagai and G. Christou, Chem. Soc. Rev., 2009, 38, 1011–1026.
- 2 R. Sessoli, D. Gatteschi, A. Caneschi and M. A. Novak, *Nature*, 1993, 365, 141.
- 3 L. Bogani and W. Wernsdorfer, Nat. Mater., 2008, 7, 179.
- 4 E. Moreno-Pineda, C. Godfrin, F. Balestro, W. Wernsdorfer and M. Ruben, Chem. Soc. Rev., 2018, 47, 501–513.
- 5 S. Demir, I.-R. Jeon, J. R. Long and T. D. Harris, Coord. Chem. Rev., 2015, 289–290, 149–176.

- 6 J. D. Rinehart, M. Fang, W. J. Evans and J. R. Long, J. Am. Chem. Soc., 2011, 133, 14236–14239.
- 7 I.-R. Jeon, J. G. Park, D. J. Xiao and T. D. Harris, J. Am. Chem. Soc., 2013, 135, 16845–16848.
- 8 (a) T. J. Woods, M. F. Ballesteros-Rivas, S. M. Ostrovsky, A. V. Palii, O. S. Reu, S. I. Klokishner and K. R. Dunbar, *Chem. Eur. J.*, 2015, 21, 10302–10305; (b) T. J. Woods, H. D. Stout, B. S. Dolinar, K. R. Vignesh, M. F. Ballesteros-Rivas, C. Achim and K. R. Dunbar, *Inorg. Chem.*, 2017, 56, 12094–12097; (c) B. S. Dolinar, S. Gomez-Coca, D. I. Alexandropoulos and K. R. Dunbar, *Chem. Commun.*, 2017, 53, 2283–2286; (d) D. I. Alexandropoulos, B. S. Dolinar, K. R. Vignesh and K. R. Dunbar, *J. Am. Chem. Soc.*, 2017, 139, 11040–11043; (e) B. S. Dolinar, D. I. Alexandropoulos, K. R. Vignesh, T. A. James and K. R. Dunbar, *J. Am. Chem. Soc.*, 2018, 140, 908–911.
- (a) K. C. Gordon, A. H. R. Al-Obaidi, P. M. Jayaweera, J. J. McGarvey, J. F. Malone and S. E. J. Bell, J. Chem. Soc., Dalton Trans., 1996, 1591–1596; (b) A. Hasheminasab, J. T. Engle, J. Bass, R. S. Herrick and C. J. Ziegler, Eur. J. Inorg. Chem., 2014, 2643–2652; (c) P. Alborés, C. Plenk and E. Rentschler, Inorg. Chem., 2012, 51, 8373–8384; (d) B. Floris, M. P. Donzello, C. Ercolani and E. Viola, Coord. Chem. Rev., 2017, 347, 115–140.
- P. Richardson, D. I. Alexandropoulos, L. Cunha-Silva, G. Lorusso, M. Evangelisti, J. Tang and T. C. Stamatatos, *Inorg. Chem. Front.*, 2015, 2, 945–948.
- (a) W. Liu and H. H. Thorp, *Inorg. Chem.*, 1993, 32, 4102–4105;
 (b) I. D. Brown and D. Altermatt, *Acta Crystallogr., Sect. B: Struct. Sci.*, 1985, 41, 244–247.
- 12 P.-H. Lin, N. C. Smythe, S. I. Gorelsky, S. Maguire, N. J. Henson, I. Korobkov, B. L. Scott, J. C. Gordon, R. T. Baker and M. Murugesu, J. Am. Chem. Soc., 2011, 133, 15806–15809.
- 13 N. F. Chilton, R. P. Anderson, L. D. Turner, A. Soncini and K. S. Murray, J. Comput. Chem., 2013, 34, 1164-1175.
- 14 X. Ma, E. A. Suturina, S. De, P. Négrier, M. Rouzières, R. Clérac and P. Dechambenoit, *Angew. Chem., Int. Ed.*, 2018, 57, 7841–7845.
- 15 J. A. DeGayner, I.-R. Jeon and T. D. Harris, Chem. Sci., 2015, 6, 6639–6648.
- 16 J. O. Moilanen, N. F. Chilton, B. M. Day, T. Pugh and R. A. Layfield, Angew. Chem., Int. Ed., 2016, 55, 5521-5525.
- 17 S. Fortier, J. J. Le Roy, C.-H. Chen, V. Vieru, M. Murugesu, L. F. Chibotaru, D. J. Mindiola and K. G. Caulton, *J. Am. Chem. Soc.*, 2013, 135, 14670–14678.
- 18 (a) I. A. Gass, C. J. Gartshore, D. W. Lupton, B. Moubaraki, A. Nafady, A. M. Bond, J. F. Boas, J. D. Cashion, C. Milsmann, K. Wieghardt and K. S. Murray, *Inorg. Chem.*, 2011, 50, 3052–3064; (b) I. A. Gass, S. Tewary, A. Nafady, N. F. Chilton, C. J. Gartshore, M. Asadi, D. W. Lupton, B. Moubaraki, A. M. Bond, J. F. Boas, S.-X. Guo, G. Rajaraman and K. S. Murray, *Inorg. Chem.*, 2013, 52, 7557–7572; (c) I. A. Gass, S. Tewary, G. Rajaraman, M. Asadi, D. W. Lupton, B. Moubaraki, G. Chastanet, J.-F. Létard and K. S. Murray, *Inorg. Chem.*, 2014, 53, 5055–5066.
- K. S. Min, A. G. DiPasquale, J. A. Golen, A. L. Rheingold and J. S. Miller, J. Am. Chem. Soc., 2007, 129, 2360–2368.
- 20 A. E. Thorarinsdottir, R. Bjornsson and T. D. Harris, *Inorg. Chem.*, 2020, 59, 4634–4649.
- 21 (a) M. Murrie, Chem. Soc. Rev., 2010, 39, 1986–1995; (b) J. M. Frost, K. L. M. Harriman and M. Murugesu, Chem. Sci., 2016, 7, 2470–2491.
- 22 A. D. Becke, J. Chem. Phys., 1993, 98, 5648-5652.
- 23 (a) S. Gomez-Coca, E. Cremades, N. Aliaga-Alcalde and E. Ruiz, J. Am. Chem. Soc., 2013, 135, 7010-7018; (b) T. J. Woods, M. F. Ballesteros-Rivas, S. Gómez-Coca, E. Ruiz and K. R. Dunbar, J. Am. Chem. Soc., 2016, 138, 16407-16416.